1521-0111/86/1/76–85$25.00
MOLECULAR PHARMACOLOGY

http://dx.doi.org/10.1124/mol.114.091926
Mol Pharmacol 86:76–85, July 2014

An N-Terminal Threonine Mutation Produces an Efflux-Favorable, Sodium-Primed Conformation of the Human Dopamine Transporter

Rheaclare Fraser, Yongyue Chen, Bipasha Guptaroy, Kathryn D. Luderman, Stephanie L. Stokes, Asim Beg, Louis J. DeFelice, and Margaret E. Gnegy

Department of Pharmacology, University of Michigan, Ann Arbor, Michigan (R.F., B.G., K.D.L., S.L.S., A.B., M.E.G.); and Departments of Psychiatry (Y.C.) and Physiology and Biophysics (L.J.D.), Virginia Commonwealth University, Richmond, Virginia

Received February 3, 2014; accepted April 21, 2014

ABSTRACT

The dopamine transporter (DAT) reversibly transports dopamine (DA) through a series of conformational transitions. Alanine (T62A) or aspartate (T62D) mutagenesis of Thr62 revealed T62D-human (h)DAT partitions in a predominately efflux-preferring conformation. Compared with wild-type (WT), T62D-hDAT exhibits reduced [^{3}H]DA uptake and enhanced baseline DA efflux, whereas T62A-hDAT and WT-hDAT function in an influx-preferring conformation. We now interrogate the basis of the mutants' altered function with respect to membrane conductance and Na^+ sensitivity. The hDAT constructs were expressed in *Xenopus* oocytes to investigate if heightened membrane potential would explain the efflux characteristics of T62D-hDAT. In the absence of substrate, all constructs displayed identical resting membrane potentials. Substrate-induced inward currents were present in oocytes expressing WT- and T62A-hDAT but not T62D-hDAT, suggesting equal bidirectional ion flow through T62D-hDAT. Utilization of the fluorescent DAT substrate ASP^+ [4-(4-(dimethylamino)styryl)-*N*-methylpyridinium] revealed that T62D-hDAT accumulates substrate in human embryonic kidney (HEK)-293 cells when the substrate is not subject to efflux. Extracellular sodium (Na^+_e) replacement was used to evaluate sodium gradient requirements for DAT transport functions. The EC_{50} for Na^+_e stimulation of [^{3}H]DA uptake was identical in all constructs expressed in HEK-293 cells. As expected, decreasing $[Na^+]_e$ stimulated [^{3}H]DA efflux in WT- and T62A-hDAT cells. Conversely, the elevated [^{3}H]DA efflux in T62D-hDAT cells was independent of Na^+_e and commensurate with [^{3}H]DA efflux attained in WT-hDAT cells, either by removal of Na^+_e or by application of amphetamine. We conclude that T62D-hDAT represents an efflux-willing, Na^+-primed orientation—possibly representing an experimental model of the conformational impact of amphetamine exposure to hDAT.

Introduction

The dopamine transporter (DAT) has a critical role in the regulation of dopamine (DA) neurotransmission because of its primary function of taking released DA from the extracellular space back into the presynaptic nerve terminal. DAT is additionally the site of action for therapeutic and abused psychostimulants such as methylphenidate, amphetamine (AMPH), and cocaine (Levi and Raiteri, 1993; Leviel, 2011). AMPH is a competitive DAT substrate that, upon translocation into the terminal, is reported to release DA from synaptic vesicles, induce reverse transport, and subsequently increase extracellular DA (Sulzer et al., 2005).

The DAT is a member of the SLC6 family of transporters that require sodium and chloride ions for substrate translocation. The electrochemical gradient of Na^+ provides the energy required to move substrate through the transporter against its concentration gradient (Chen et al., 2004b; Hahn and Blakely, 2007). The alternate access model is the common paradigm for the translocation of neurotransmitter and cotransported ions (Jardetzky, 1966), in which the transporter transitions between open-outward to open-inward orientations to move substrate from outside to inside the cell. Crystallization of the leucine transporter (LeuT), a bacterial SLC6 homolog (Yamashita et al., 2005; Krishnamurthy and Gouaux, 2012), provided considerable information about the Na^+ symporter structure and translocation mechanisms that further validate the alternate access model. DAT also generates unexpectedly large currents, and evidence exists for a channel mode of conduction (Ingram et al., 2002; Carvelli et al., 2004, 2008; DeFelice and Goswami, 2007). Elegant molecular modeling comparisons of LeuT to human (h)DAT

This work was supported by the National Institutes of Health National Institute on Drug Abuse [Grants 5R01-DA011697 (to M.E.G.), 5RC1-DA028112 and 5R01-DA026947 (to L.J.D.), and 5T32-DA007281 (to R.F.)].
R.F. and Y.C. contributed equally to this work.
dx.doi.org/10.1124/mol.114.091926.

ABBREVIATIONS: AMPH, amphetamine; ANOVA, analysis of variance; ASP^+, 4-(4-(dimethylamino)styryl)-*N*-methylpyridinium); CI, confidence interval; cRNA, capped RNA; DA, dopamine; DAT, dopamine transporter; HEK, human embryonic kidney cells; GBR12935, 1-[2-(diphenylmethoxy) ethyl]-4-(3-phenylpropyl)-piperazine; KRH, Krebs-Ringer HEPES buffer; LeuT, leucine transporter; MPP^+, 1-methyl-4-phenylpyridinium; Na^+_e, extracellular sodium; NMDG-Cl, *N*-methyl-D-glucamine chloride; RMP, resting membrane potential; TM, transmembrane domain; WIN 35,428, (−)-2-β-carbomethoxy-3-β-(4-fluorophenyl)tropane-1,5-napthalenedisulfonate; WT, wild-type.

have identified fundamental transmembrane domains (TM) and amino acid residues involved in ligand binding and the extracellular-to-intracellular translocation of substrate (Zhao et al., 2010, 2012; Shan et al., 2011). However, the mechanisms regulating the binding of DA and cotransported ions during intracellular-to-extracellular transport are less understood.

The DAT N terminus contains various serine and threonine residues that are important for the regulation of transporter activity (Foster et al., 2002) and AMPH-induced DA efflux (Khoshbouei et al., 2004; Foster et al., 2012). We investigated the putatively phosphorylated threonine residue within the highly conserved RETW sequence of the DAT N terminus (Vaughan, 2004) for its role in the mechanisms of AMPH. The RETW sequence is juxtaposed to the TM1a segment (Yamashita et al., 2005), which is within a DAT region identified as the intracellular gating network (Kniazeff et al., 2008). Conservative (alanine, A) and nonconservative (aspartate, D) mutations were introduced at the Thr62 residue, which also mimic a nonphosphorylated (T62A) and a phosphorylated (T62D) state (Guptaroy et al., 2009). Compared with wild-type (WT) human (h)DAT, T62D-hDAT human embryonic kidney (HEK) cells demonstrated a reduction in the uptake of [^{3}H]DA with a concomitant increase in the rate of basal DA release (Guptaroy et al., 2009). Moreover, T62D-hDAT was insensitive to AMPH. These functions were rescued when measured in the presence of zinc, which has been used to correct dysfunctions of other intracellular-favoring hDAT mutants (Loland et al., 2002; Meinild et al., 2004). The phenotype of T62A-hDAT cells showed greater similarity to WT, with a reduction in both DA influx and AMPH-stimulated DA efflux. Additional studies revealed an enhanced affinity for DAT substrates in the T62-hDAT mutants (Guptaroy et al., 2011), particularly in the T62D-hDAT HEK cells. Enhanced substrate affinity can occur when the transition of substrate-bound transporter from the intracellular (inward)-to-extracellular (outward) orientation is kinetically favored (Chen et al., 2004a; Guptaroy et al., 2009, 2011).

In this study we used the T62D-hDAT to further investigate the influence of transporter orientation on the membrane potential and the requirements of Na^+ in DAT functions. We examined if the elevated basal DA efflux measured in T62D-hDAT HEK cells could be attributed to 1) poor intracellular accumulation of substrate, 2) an intrinsic depolarization of the cell membrane, or 3) a modification in requirement for the Na^+ gradient. These hypotheses were tested using a combination of electrophysiology measurements in *Xenopus* oocytes and radioligand and fluorescent microscopy techniques in heterologous cells. The results from these experiments strengthened the conclusion that T62D-hDAT partitions in a conformation that represents an inward-favorable "Na^+-primed" state able to maximize DA efflux.

Materials and Methods

Construction and Expression of WT and Thr62-hDAT Mutants in *Xenopus* Oocytes. Restriction enzyme sites for 5′ NotI and 3′ XbaI were added to the flag-tagged WT and Thr62-hDAT mutant DNA constructs (Guptaroy et al., 2009) and subcloned into the pSGEM *Xenopus* oocyte expression vector. After linearization of the plasmid with SbfHI-HF digestion (New England BioLabs Inc., Ipswich, MA), capped RNA (cRNA) was prepared according to protocol with the mMessage mMachine T7 kit (Ambion Inc., Ausin, TX). *Xenopus* oocyte preparation was described previously (Solis et al., 2012). Stage IV–V oocytes were microinjected with 25 nl water or 25 ng (1 ng/nl) hDAT cRNA using a Nanoject autoinjector (Drummond Scientific, Broomall, PA). Oocytes were incubated at 18°C in Super Barth's solution, pH 7.4 [in mM: 88 NaCl, 1 KCl, 0.33 $Ca(NO_3)_2 \cdot 4H_2O$, 0.41 $CaCl_2 \cdot 2H_2O$, 1 $MgSO_4 \cdot 7H_2O$, 2.4 $NaHCO_3$, 10 HEPES, 1 Na-Pyruvate, and 50 mg/ml gentamicin] for 4–8 days before electrophysiology recordings.

Electrophysiology Measurements in *Xenopus* Oocytes Expressing WT and Thr62 Mutant hDAT. Whole-cell currents or membrane potentials were measured by two-electrode voltage clamp techniques using a GeneClamp 500 (Molecular Devices, Palo Alto, CA). A 16-bit A/D converter (Digidata 1322A; Molecular Devices) interfaced to a PC running Clampex 10 (Molecular Devices) was used to control membrane voltage and acquire data. Microelectrodes were pulled using a programmable puller (Model P-87; Sutter Instrument Company, Novato, CA) to a resistance of 1.0–5.0 MΩ when filled with 3.0 M KCl electrode solution. Unless otherwise noted, oocytes were voltage clamped at –60 mV. Current was recorded continuously or with a step-voltage protocol. The perfusion solutions were changed by a gravity-driven perfusion system at a rate of 1 ml/min. Oocytes were bathed/perfused in the HEPES-buffered solution ND96 (in mM: 96.0 NaCl, 2.0 KCl, 1.0 $MgCl_2$, 1.8 $CaCl_2$, and 5.0 HEPES-NaOH, pH 7.5). All experiments were performed at room temperature (22–24°C).

Expression and Maintenance of WT and Thr62 Mutant hDAT HEK Cells. Wild-type-, T62A-, and T62D-mutant hDAT were cloned and stably expressed in HEK-293T cells as previously described (Guptaroy et al., 2009). Parental and hDAT HEK cells were maintained in high glucose Dulbecco's modified Eagle's medium supplemented with 10% fetal bovine serum and 1% penicillin/streptomycin at 37°C and 5% CO_2. All experiments utilizing hDAT HEK cells were performed with intact, attached cells at room temperature.

Measurement and Analysis of ASP^+ Accumulation with Live Cell Confocal Microscopy. Accumulation of the fluorescent substrate ASP^+ [4-(4-(dimethylamino)styryl)-*N*-methylpyridinium] (Molecular Probes, Eugene, OR) was measured with confocal imaging in live HEK cells (Schwartz et al., 2003; Zapata et al., 2007) expressing WT- and Thr62-mutant hDATs. Cells were plated on poly-D-lysine–coated, 35-mm glass bottom MatTek culture dishes (MatTek, Ashland, MA) at a density of 300,000–500,000 cells per dish 1 day prior to imaging. The culture media was aspirated and cells were washed twice in normal Krebs-Ringer HEPES (KRH) buffer, pH 7.4 [in mM: 125 NaCl, 4.8 KCl, 1.2 KH_2PO_4, 1.3 $CaCl \cdot 2H_2O$, 1.2 $MgSO_4 \cdot 7H_2O$, 5.6 glucose, and 25 HEPES] containing 50 μM pargyline (monoamine oxidase inhibitor), 1 mM tropolone (catechol-*O*-methyl transferase inhibitor), and 50 μM ascorbic acid (DA antioxidant) (Sigma-Aldrich, St. Louis, MO). Cells were incubated at 37°C in 2 ml of 5 μg/ml Hoechst nuclear stain (Molecular Probes) for 30 minutes. Then cells were washed three times quickly and then twice more for 5 minutes, each under light protection with gentle rocking. Plates were mounted on a Nikon A1R (Nikon Instruments, Inc., Melville, NY) confocal microscope with a 60× 1.4–numerical aperture oil objective. Cell boundaries were confirmed with a differential interference contrast (DIC) image. Images were gathered 1 μm beyond the cell center, determined by the nuclear stain, to increase the accumulation measured within the cytosolic space. A test plate of WT-hDAT HEK cells was used to set the levels for intensity, brightness, and contrast for minimal saturation of the fluorescent signal of each laser channel. These microscope settings were not adjusted during the image acquisition of experiment plates. The Hoechst stain was excited with a UV laser at 405 nm and emission measured between 425 and 475 nm. ASP^+ was excited using the Cy3.5 laser with excitation at 561 nm and emission at 570–620 nm. Images were acquired at room temperature with a time scan every 10 seconds for 3 minutes. ASP^+ (2 μM, 2 ml) was carefully added to the cells after the first 10-second acquisition. The optical density within whole cell regions was quantified using ImageJ software (NIH,

Bethesda, MD). Data are expressed as the optical density measured within the cell across time. By the end of image acquisition (3 minutes), the background fluorescence in parental HEK cells was around 60% of the ASP^+ fluorescent signal in HEK cells expressing WT or Thr62 mutant hDATs.

ASP^+ Competition of Radiolabeled Dopamine and WIN 35,428. Radioligand competition experiments were similar to assays described previously (Guptaroy et al., 2009, 2011). Cells were seeded onto 24-well plates at a density of 200,000 cells per well 1 day before the experiment. Uptake of 10 nM [^{3}H]DA (specific activity, 46 Ci/mmol) for 3 minutes or displacement of [^{3}H]WIN 35,438 [(−)-2-β-carbomethoxy-3-β-(4-fluorophenyl)tropane-1,5-napthalenedisulfonate] (specific activity, 85 Ci/mmol) binding for 30 minutes (PerkinElmer Life and Analytical Sciences, Waltham, MA) were measured at room temperature with ASP^+ at concentrations ranging from 0 to 1 mM (prepared in KRH buffer containing 10% dimethyl sulfoxide). Nonspecific [^{3}H]DA uptake or [^{3}H]WIN 35,438 binding was determined in the presence of 100 μM cocaine or 5 μM GBR12935 (1-[2-(diphenylmethoxy)ethyl]-4-(3-phenylpropyl)-piperazine), respectively, following a 10-minute preincubation with the inhibitor alone. At the end of the assay, cells were washed four times in ice-cold phosphate-buffered saline then lysed in 0.25 ml 1% SDS. Radioactivity was measured in 5 ml of ScintiVerse cocktail (Thermo Fisher Scientific, Waltham, MA) using a Beckman LS5801 scintillation counter (Beckman Coulter, Brea, CA).

Extracellular Sodium Substitution. For experiments involving changes in concentrations of extracellular sodium, NaCl in the KRH buffer was replaced with corresponding concentrations of *N*-methyl-D-glucamine chloride (NMDG-Cl). [^{3}H]DA uptake was measured as described above with varying levels of extracellular sodium (Na^+_e). Assay buffer with 0, 10, 30, 50, 100, and 125 mM NaCl contained 125, 115, 95, 75, 25, and 0 mM NMDG-Cl, respectively. Maximum uptake was obtained in the normal 125-mM NaCl condition for all constructs.

For DA efflux experiments, cells were preloaded with 0.5 μM DA (containing 15 nM [^{3}H]DA) in normal KRH. After washing, 0.25 ml of fresh Na^+-substituted KRH was collected and replaced for 15 minutes to evaluate the baseline DA efflux. The effect of Na^+_e on AMPH-induced DA release was determined after a 5-minute application of 10 μM AMPH, followed by collection of an additional 5-minute aliquot at 20 minutes. At the end of the assay, cells were solubilized to measure the final amount of DA remaining inside of the cells after efflux. Total [^{3}H]DA after preloading was calculated as the sum of radioactivity in all efflux fractions and final intracellular DA. Basal DA efflux was calculated as a percentage of the calculated total [^{3}H]DA. AMPH-induced [^{3}H]DA efflux was calculated as a percentage of the total [^{3}H]DA inside the cell prior to the AMPH treatment.

Statistical Analysis. The electrophysiological data were analyzed with Clampfit 10 (Molecular Devices) and Origin 8 (OriginLab, Northampton, MA). Statistical differences were determined by one-way analysis of variance (ANOVA) with Tukey's multiple comparisons test or unpaired *t* test with Welch's correction using GraphPad Prism 6 software (GraphPad Software, San Diego, CA). Dose-response curves were analyzed with GraphPad Prism 6 software to determine the IC_{50} and EC_{50} values for [^{3}H]DA uptake competition by nonlinear regression analyses. Statistical differences were compared between constructs by testing whether the null hypothesis of the parameter was the same between all data sets. A rejection of the null hypothesis indicated a statistical difference between the comparisons (*P* value was below 0.05). Values are provided plus or minus S.E.M. along with the 95% confidence intervals. Statistical differences for ASP^+ accumulation between cell types were determined by two-way ANOVA with Tukey's multiple comparisons test at each time point.

Results

Electrophysiologic Properties of hDAT Mutants. DAT is an electrogenic transporter, and current through the transporter in excess of the fixed stoichiometry of 1:2:1 for Cl^-:Na^+:DA has been detected (Sonders et al., 1997). Moreover, DAT-mediated DA efflux is greater at depolarized potentials (Khoshbouei et al., 2003). We posited that the changes in uptake and efflux of DA in the T62-hDAT mutants (Guptaroy et al., 2011) could correspond to altered electrophysiological properties. Therefore, we conducted electrophysiological studies of the hDAT and T62-hDAT mutants to supplement or disprove this hypothesis. The cRNAs for the mutants were transfected into *Xenopus* oocytes because transporter-mediated currents are large in these cells and much easier to measure than in cultured cells.

Xenopus oocytes were injected with equal amounts of hDAT cRNA for the three constructs. The DAT expression was confirmed by [^{3}H]DA uptake assays in five individual oocytes. DA uptake in hDAT-expressing oocytes was approximately 40% greater than in control water-injected oocytes 4 days after cRNA injections (data not shown). The resting membrane potentials (RMP) were measured in oocytes expressing the transporters and are summarized in Fig. 1. The RMP in control oocytes was approximately –40 mV (–41.5 ± 2.6 mV). Expression of WT, T62A, or T62D hDAT caused significant depolarization of the RMP to approximately –25 mV (WT-hDAT, –25.3 ±1.5 mV; T62A-hDAT, –27.0 ±1.4 mV; and T62D-hDAT, –24.3 ± 1.1 mV), which was statistically different from the RMP in control oocytes (control versus WT and T62D, $P < 0.0001$; control versus T62A, $P = 0.0014$). However, the level of depolarization induced by T62A- or T62D-hDAT expression in the oocytes was not different from that of WT-hDAT oocytes. The well characterized leak current present in DAT in the absence of substrate (Sonders et al., 1997) probably accounts for the depolarization of the oocyte. Therefore, the baseline current passing through the transporter in the absence of substrate is not affected by the Thr62 mutations.

DAT substrates such as DA and AMPH induce inward currents that are primarily attributed to an inward flux of Na^+ ions (Sonders et al., 1997). The substrate-induced currents in oocytes expressing WT-, T62A-, and T62D-hDAT were recorded

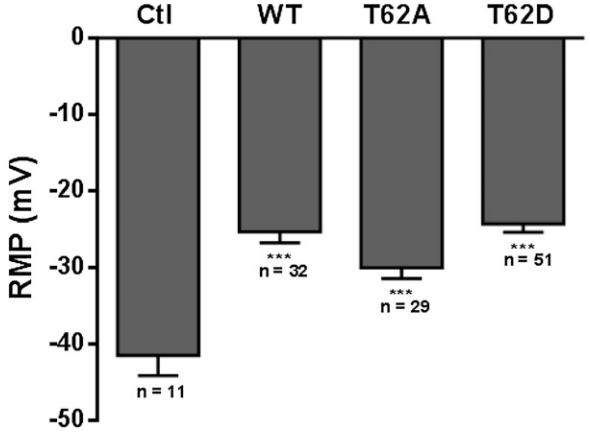

Fig. 1. Expression of WT-, T62A-, and T62D-mutant hDATs causes similar membrane depolarization in *Xenopus* oocytes. *Xenopus* oocytes were injected with 23 ng of cRNA for WT-, T62A-, or T62D-hDAT. Expression of hDAT statistically reduces the recorded RMP of oocytes when compared with control oocytes (Ctl) injected with 23 nl or water (***$P < 0.001$).

with a holding potential of –60 mV. Representative trace recordings from oocytes are shown in Fig. 2A and the changes in accumulated current in WT-, T62A-, and T62D-hDAT oocytes held at –60 mV are shown in Fig. 2B. Currents were measured after the application of 10 μM DA for 1 minute. DA produced inward currents in oocytes expressing WT-hDAT and T62A-hDAT that were absent in control oocytes lacking the transporter. The fast phase of the inward current lasted less than 10 seconds followed by a slow recovery phase. The change in current before and after DA application was –6.60 ± 1.53 nA in WT-hDAT, –3.85 ± 0.38 nA in T62A-hDAT, and –0.34 ± 0.30 in T62D-hDAT. Negligible current was measured in response to DA in the T62D-hDAT oocytes. These results correspond with our previous reports of a substantial reduction in the V_{max} for [^{3}H]DA uptake in T62A-hDAT HEK293 cells compared with WT-hDAT HEK293 cells (Guptaroy et al., 2009). Similar results were recorded with the application of AMPH (data not shown). Membrane conductance was next measured with a step-voltage protocol and the current difference is plotted in Fig. 3. Whereas membrane conductance was observed with DA application to WT- and T62A-hDAT oocytes (Fig. 2, A and C), the current-voltage curves confirmed there was no change in conductance with the application of DA (Fig. 3C) or AMPH (data not shown) in T62D-hDAT oocytes. T62D-hDAT is expressed at the oocyte plasma membrane, since [^{3}H]DA uptake experiments from different oocytes confirmed expression and function of T62D-hDAT. Zinc has been used to improve transport in T62D-hDAT HEK293 cells (Guptaroy et al., 2009, 2011) and other uptake-defective DAT mutant transporters (Loland et al., 2002; Chen et al., 2004a). Binding of zinc stabilizes a conformation of DAT that increases chloride conductance (Loland et al., 2002; Meinild et al., 2004). The use of zinc was employed to further validate the function of T62D-hDAT–expressing oocytes. Coapplication of DA and 2 μM $ZnCl_2$ after treatment of DA alone in the same T62D-hDAT oocyte produced a measurable substrate-induced current (Fig. 2A). Although Zn^{2+} per se induced small inward currents in each transcript, as seen in Figs. 2B and 3, it significantly potentiated the DA-induced inward current measured at –60 mV in the hDAT oocytes (comparison of values, DA ± zinc: WT-hDAT, $P = 0.02$; T62A-hDAT, $P < 0.0001$; and T62D-hDAT, $P = 0.0003$). These data not only provided functional evidence for the membrane expression of T62D-hDAT but demonstrated that the defective gating of the T62D-hDAT mutant could be partially rescued by zinc. As the holding potential became higher than the reversal potential, outward currents in all the hDAT constructs were similar with the application of zinc alone or in combination with DA. Outward currents at depolarizing potentials were not observed without application of zinc (Fig. 3).

Affinity and Accumulation of the Fluorescent Substrate ASP$^+$ in WT- and Thr-hDAT Mutant HEK Cells. In previous studies (Guptaroy et al., 2009), we found that T62D-hDAT demonstrated high affinity, but very low V_{max}, for [^{3}H]DA uptake with high basal efflux. We postulated that substrate would not accumulate intracellularly because of the accelerated outward transport. K_m and V_{max} values for [^{3}H]DA uptake for T62A-hDAT were intermediate between T62D-hDAT and WT (Guptaroy et al., 2009). To test this explanation, we conducted uptake experiments with the three constructs expressed in HEK cells using the fluorescent monoamine transporter substrate ASP$^+$. ASP$^+$ is structurally similar to the dopaminergic neurotoxin MPP$^+$ (1-methyl-4-phenylpyridinium). ASP$^+$ is taken up normally through the transporters, but because of intracellular binding to mitochondria, it is not available for efflux (Schwartz et al., 2003).

Uptake and binding of the ASP$^+$ substrate to the WT- and Thr62-mutant hDAT HEK constructs were confirmed with radioligand competition assays. Dose-response curves for ASP$^+$ competition of [^{3}H]DA uptake (Fig. 4A) and displacement of the cocaine analog [^{3}H]WIN 35,428 (Fig. 4B) did not differ among WT- and Thr62-hDAT mutant cell lines. The IC_{50} values (μM) (with 95% confidence intervals) for ASP$^+$ competition of [^{3}H]DA uptake were 11.95 (8.87–16.1) in WT-, 17.60 (10.6–29.2) in T62A-, and 12.08 (10.3–14.1) in T62D-hDAT HEK cells (Fig. 4A). ASP$^+$ inhibited [^{3}H]WIN 35,428 binding with IC_{50} (μM) values of 11.95 (8.87–16.1) in

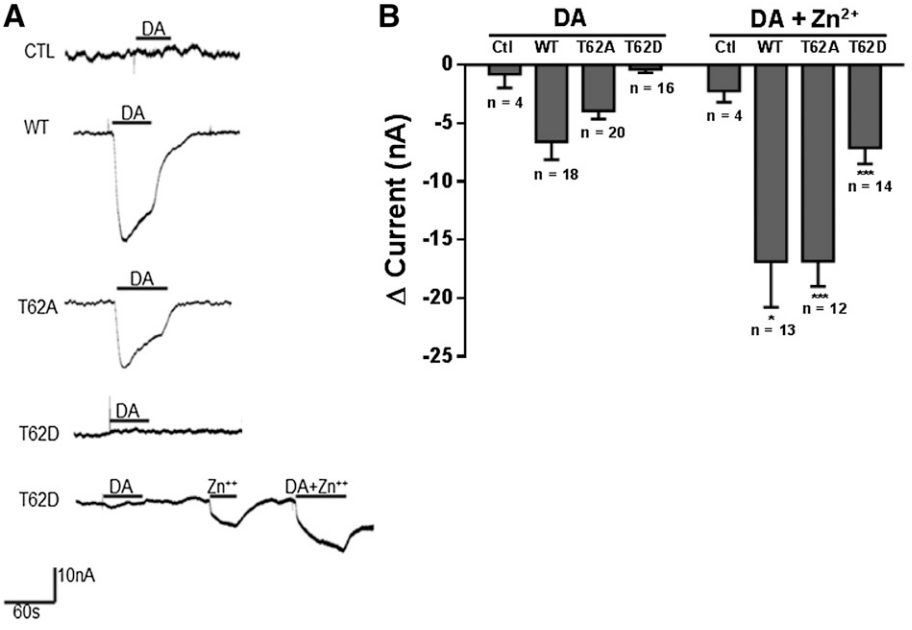

Fig. 2. Dopamine-induced inward currents in T62D-hDAT oocytes are partially rescued by zinc. (A) Representative continuous traces of currents measured in oocytes clamped at –60 mV are shown. Inward currents are observed in WT- and T62A-hDAT oocytes after application of 10 μM DA. Coapplication of 2 μM $ZnCl_2$ partially restored a measurable inward current in T62D-hDAT oocytes. (B) Change in accumulated current (Δ current = DA current – baseline current) in WT-, T62A-, and T62D-hDAT oocytes held at –60 mV. The data are expressed as the average ± S.E.M with numbers of oocytes for each condition given. Unpaired t test with Welch's correction for DA ± zinc application shows a significant increase in the DA-induced currents in WT- (*$P < 0.05$), T62A- (***$P < 0.001$), and T62D-hDAT (***$P < 0.001$)–expressing oocytes. Zinc did not affect the DA current measurement in control oocytes. Ctl, control.

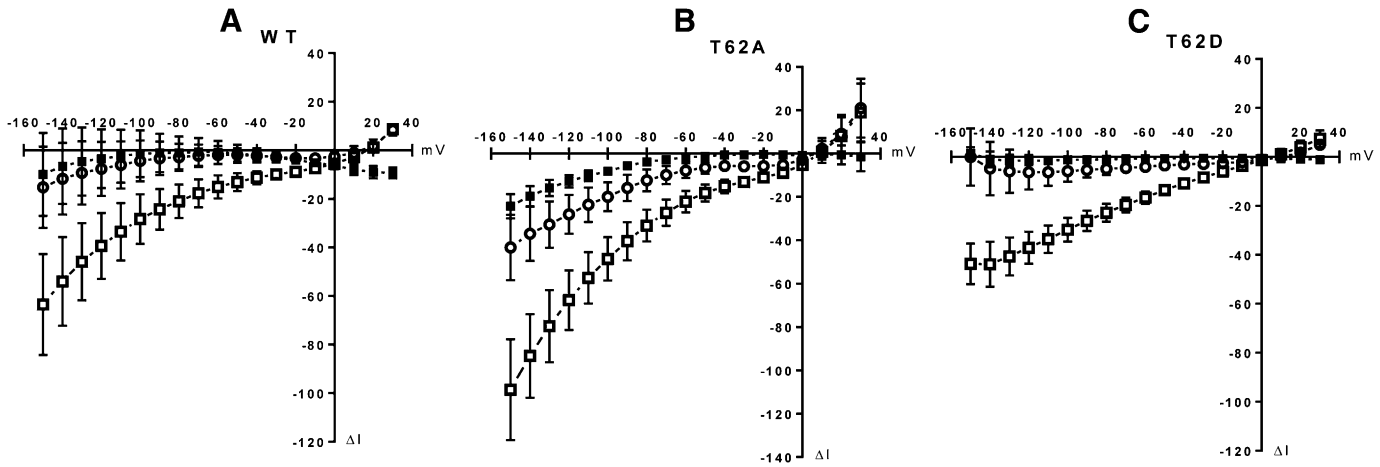

Fig. 3. Current-voltage relationships in hDAT-expressing *Xenopus* oocytes. A step–voltage clamp protocol was used from –150 to 30 mV at a holding potential of –60 mV and with 10-mV step increments for a 30-second duration at each step. Oocytes were challenged with 10 μM DA ± 2 μM $ZnCl_2$. The current is displayed as the difference from baseline measured in the absence of substrate (ΔI). At hyperpolarizing potentials, DA (■) induces an inward current in (A) WT- and (B) T62A-hDAT oocytes. Coapplication with zinc (□) potentiates DA-induced inward currents. (C) In T62D-hDAT oocytes, DA inward currents are only measurable in the presence of zinc. Application of zinc alone (○) produced a small current in all constructs. Each current-voltage plot was generated from four to six oocytes expressing the indicated hDAT construct.

WT-, 18.6 (10.6–29.2) in T62A-, and 12.1 (10.3–14.1) in T62D-hDAT HEK cells (Fig. 4B).

Using fluorescence microscopy, we measured uptake of ASP^+ (Fig. 5). There was a low level of background fluorescence prior to the addition of ASP^+ which did not differ among cell types. However, the fluorescence intensity increased with time after cells containing the DAT constructs were exposed to 2 μM of ASP^+. Representative confocal images prior to (time 0) and after (3 minutes) ASP^+ addition are shown for WT-, T62A-, T62D-hDAT, and parental HEK-293T cells in Fig. 5, A–D. The full time course of intracellular ASP^+ accumulation in each cell type is shown in Fig. 5E. There was no difference in ASP^+ uptake among WT-, T62A-, and T62D-hDAT cells, but ASP^+ uptake in the three DAT-containing cell lines was significantly different from that in parental HEK cells at all time points [$P < 0.0001$ for genotype, $F(3, 558) = 54.06$; time $F(19, 10602) = 2360$, and interaction between genotype and time, $F(57, 10602) = 31.37$]. The linear rate of ASP^+ uptake in O.D. units/s during the first 30 seconds (95% confidence interval [CI]) was 0.123 (0.109–0.137) for WT-hDAT, 0.110 (0.096–0.125) for T62A-hDAT, and 0.103 (0.089–0.116) for T62D-hDAT versus 0.043 (0.032–0.053) in parental HEK cells. The uptake rate in the parental HEK cells significantly differed from the cells containing the three DAT constructs at $P < 0.0001$, $F = 29.7246$, $DF_n = 3$, $DF_d = 2240$.

To demonstrate that the results with uptake of ASP^+ were attributable to the T62D mutation and not the substrate itself, we performed uptake and efflux experiments with [^{3}H]MPP^+ in WT- and T62D-hDAT cells. [^{3}H]MPP^+ is structurally similar to ASP^+ but is readily subject to reverse transport through DAT. Results are highly similar to those using [^{3}H]DA (Guptaroy et al., 2009). The uptake of [^{3}H]MPP^+ in pmol/min per milligram protein (with 95% CI) was 260 (222–297) in WT-hDAT cells versus 8.4 (5.8–10.9) in T62D-hDAT cells [$P < 0.0005$, $F = 45.7$ (1,6)] for an experiment performed in triplicate. The linear rate of [^{3}H]MPP^+ efflux, in pmol [^{3}H]MPP^+/μM intracellular [^{3}H]MPP^+ (95% CI), is 6.5 (4.3–8.5) for WT cells and 24.9 (22.5–27.3) for T62D-hDAT cells [$P = 0.00067$, $F = 91.3$ (1,4)].

Differential Sodium Requirements for DA Uptake Versus Efflux in T62D-hDAT Mutants. Given our findings of identical intracellular ASP^+ retention among the DAT constructs despite differences in substrate-induced membrane conductance, we next explored the effect of Na^+ on the function of T62D-hDAT compared with the other constructs. To determine whether the Thr62 mutations would alter the Na^+ requirements for hDAT function, we measured [^{3}H]DA uptake and efflux in WT-, T62A-, and T62D-hDAT HEK cells while varying the extracellular concentrations of Na^+ [Na^+_e]. NaCl was replaced with NMDG-Cl to maintain osmolarity of

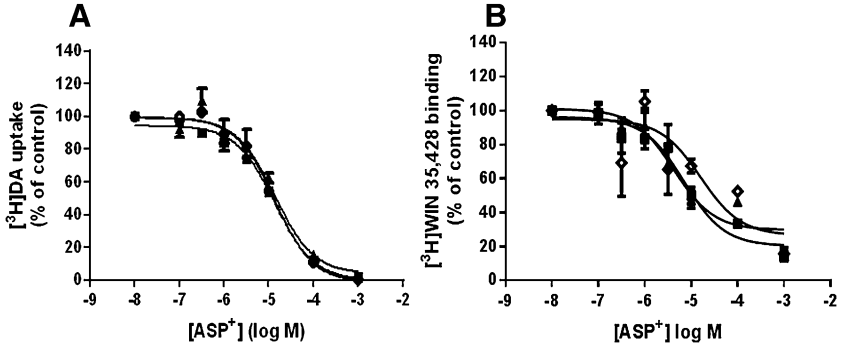

Fig. 4. Affinity of the fluorescent substrate ASP^+ is unaffected by the T62A- or T62D-hDAT mutations. As detailed in *Materials and Methods*, (A) uptake of 10 nM [^{3}H]DA for 3 minutes or (B) binding of [^{3}H]WIN 35,428 for 30 minutes in WT- (■), T62A- (▲), and T62D-(◇) hDAT HEK cells was measured as a function of varying ASP^+ concentrations. Data are expressed as the percent of the control without ASP^+ and are shown as the mean ± S.E.M; $n = 2$ experiments performed in triplicate. The IC_{50} (μM) values with 95% confidence intervals are reported in *Results*.

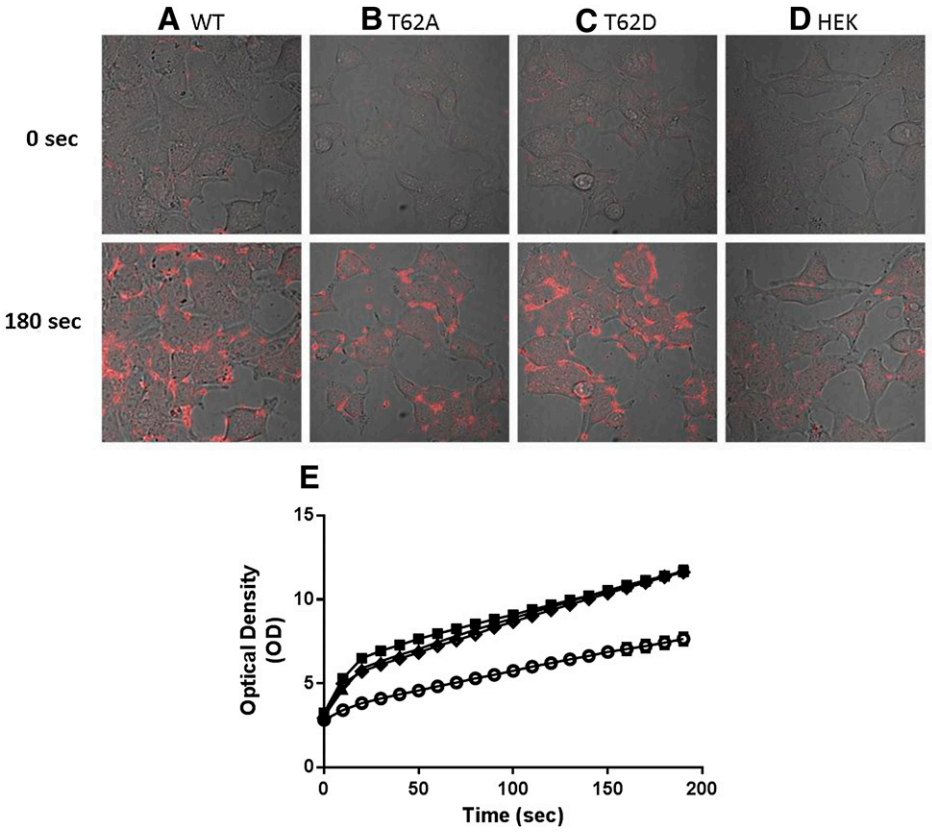

Fig. 5. Accumulation of fluorescent substrate ASP^+ in T62A- and T62D-hDAT HEK cells. Representative confocal images of time-dependent ASP^+ accumulation are displayed in columns (A) WT-, (B) T62A-, and (C) T62D-hDAT, and (D) parental HEK cells. Acquired representative images of differential interference contrast and ASP^+ signals are overlain, at times 0 and 180 seconds after exposure to 2 μM ASP^+. (E) The optical density of the fluorescent signal was quantified in intracellular regions of WT- (■), T62A- (▲), T62D- (◊) hDAT, and parental (°) HEK cells using ImageJ software. Data are plotted for the full 3-minute image acquisition of 10-second intervals; WT, n = 140 cells; T62A, n = 126 cells; T62D, n = 148 cells; and HEK, n = 148 cells.

the cells. In all cell lines, there was very little uptake of [^{3}H]DA with complete NMDG-Cl substitution (0 mM Na^+_e), but [^{3}H]DA uptake increased identically in all three cell lines as the [Na^+_e] rose. There was no statistical difference between the EC_{50} [mM (95% CI)] values for Na^+ stimulation of [^{3}H]DA uptake in WT-, 39.6 (26.7–58.5); T62A-, 40.5 (29.7–55.1); or T62D-hDAT HEK cells, 58.7 (39.4–87.6) (Fig. 6).

Outward transport through DAT demonstrates an inverse dependence on Na^+_e compared with inward transport. Removal or lowering of extracellular Na^+ stimulates substrate efflux in cells expressing monoamine transporters (Pifl et al., 1997; Pifl and Singer, 1999) or brain tissue preparations (Liang and Rutledge, 1982; Raiteri et al., 1979) by shifting the internal Na^+ gradient to favor reversal of the transporter. Previously we reported that T62D-hDAT had an elevated basal leak of [^{3}H]DA, which exceeded that of WT at physiologic levels of Na^+_e (Guptaroy et al., 2009). Here, the behavior of the basal and AMPH-stimulated efflux as a function of Na^+_e was examined.

WT-hDAT HEK cells showed the expected elevation in basal [^{3}H]DA efflux upon removal of Na^+_e, and the elevation was maintained throughout the 15-minute incubation period (Fig. 7A, open bars). The baseline efflux significantly decreases as [Na^+_e] progresses from 0 to 10, 50, and 125 mM (Fig. 7A, clear, checkered, gray, and black bars; see figure legend for statistics for varied Na^+_e at individual time points). This same pattern recurred at the 10-minute and 15-minute time points (Fig. 7A, checkered, gray, and black bars). In a two-way ANOVA, there was a main effect of time [$P < 0.01$, $F_{(3, 56)} = 8.043$] and a significant interaction between [Na^+_e] and time [$P < 0.0001$, $F_{(9, 56)} = 12.80$] with no main effect of [Na^+_e] [$P = 0.08$, $F_{(3, 56)} = 3.24$]. Significant stimulation of efflux by 10 μM AMPH above the corresponding baseline is only evident at 50 mM Na^+_e ($P < 0.05$, post hoc Tukey's) and 125 mM Na^+_e ($P < 0.0001$, post hoc Tukey's) (Fig. 7A, 20 minutes). On the contrary, at 0 mM Na^+_e, 10 μM AMPH

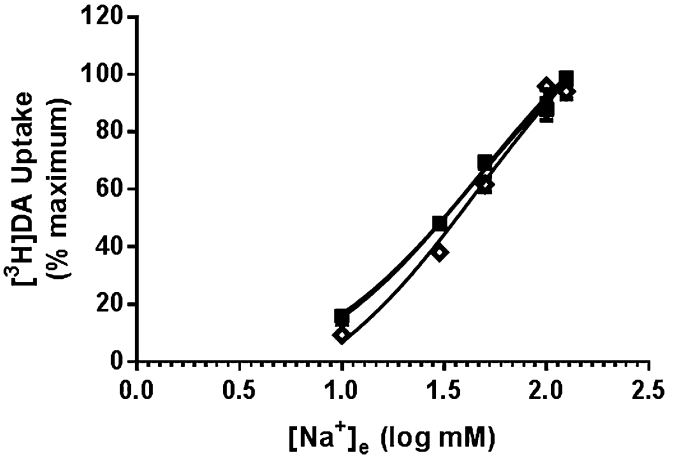

Fig. 6. The reliance on extracellular Na^+ to promote DA uptake is not altered by the Thr62-hDAT mutations. Extracellular sodium (Na^+_e) stimulation of [^{3}H]DA uptake in WT- and T62-mutant hDAT HEK cells. Uptake of 10 nM [^{3}H]DA was conducted for 3 minutes at room temperature. Na^+ in the uptake buffer was replaced with NMDG-Cl to maintain osmolarity. The IC_{50} (mM) for Na^+_e in WT- (■), T62A- (▲), and T62D- (◊) hDAT was 39.6, 40.5, and 58.7, respectively. Data are from n = 4 experiments done in triplicate and reported as a percentage of the maximum uptake achieved at the normal, highest [Na^+_e] tested.

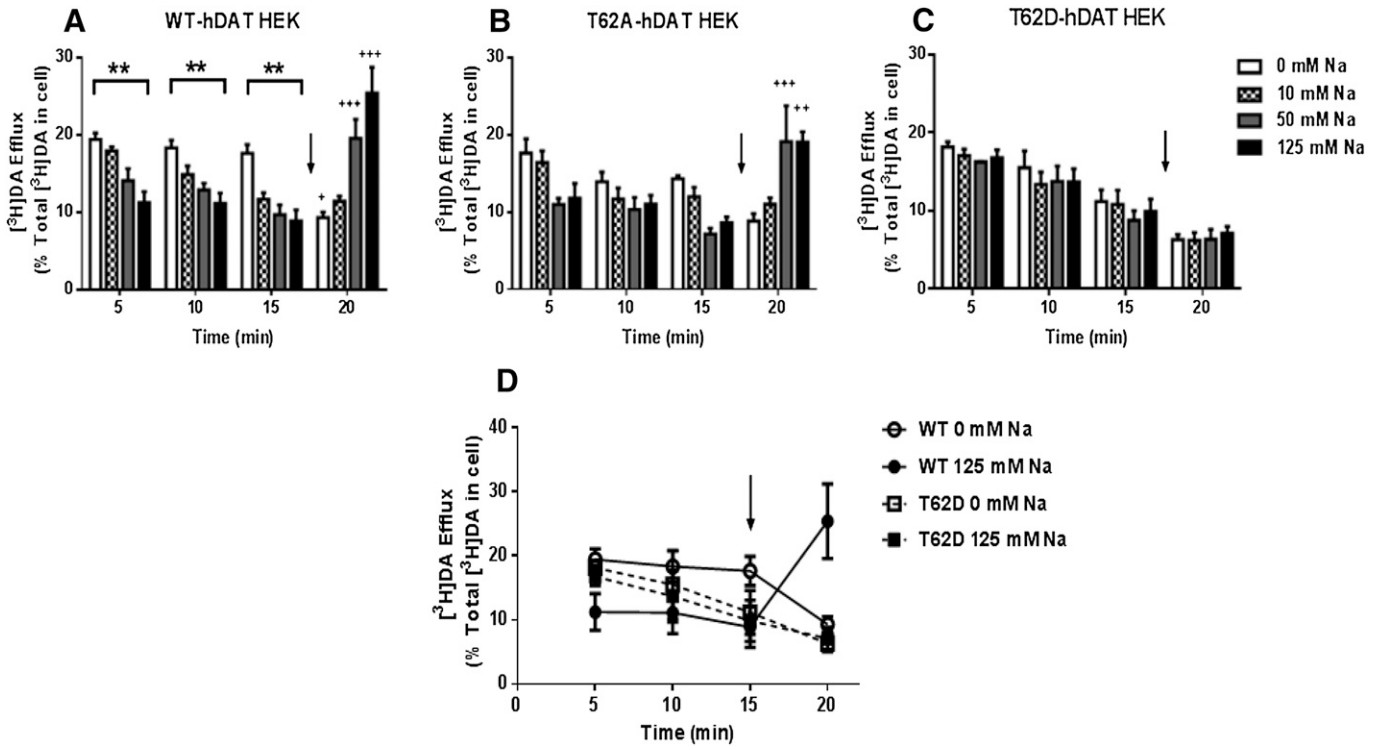

Fig. 7. Initial [^{3}H]DA efflux in T62D-hDAT is Na^+-independent and resembles inducible DA efflux of WT-hDAT HEK cells. (A) WT-, (B) T62A-, and (C) T62D-hDAT HEK cells were preloaded with 0.5 μM [^{3}H]DA (in normal KRH buffer) for 20 minutes. Basal and AMPH-induced DA efflux were determined while varying [Na^+_e]. After 15 minutes cells were stimulated with AMPH (10 μM, black arrow) while varying [Na^+_e] for 5 minutes. Data are averaged from three to six experiments performed in three or four replicates. In WT (A) and T62A (B), $^{**}P < 0.01$ for 0 versus 125 mM for basal DA efflux at times 5, 10, and 15 minutes; $^{+++}P < 0.001$; $^{++}P < 0.001$; or $^{+}P < 0.05$ for AMPH-induced DA efflux at 20 minutes compared with 15 minutes (before AMPH) at each corresponding [Na^+_e]. (D) Comparisons of basal and AMPH (black arrow) DA efflux in WT (circles) and T62D (squares) at 0 mM (open symbols) and 125 mM (closed symbols) Na^+_e. To account for variation in DA uptake, the data are represented as a percentage of the total [^{3}H]DA inside of the cell after DA preloading. Analyses of the three-way interaction (time versus [Na^+_e] versus cell type) is not significantly different between WT and T62D at 0 mM Na^+ (with the exception of 15 minutes, $P = 0.005$). DA efflux after AMPH (20 minutes) is significantly greater in WT compared with T62D at 125 mM Na^+ ($P < 0.0001$), with no difference between cell types at 0 mM Na^+ ($P = 0.23$). The effect of Na^+_e on DA efflux (time versus cell type versus [Na^+_e]) was significant in WT- ($P \leq 0.001$) but not in T62D-hDAT. Analyses of cell type versus [Na^+_e] versus time shows a significant change after the addition of AMPH (15 versus 20 minutes) in WT-hDAT at both 0 mM ($P = 0.002$) and 125 mM Na^+ ($P < 0.0001$); and in T62D-hDAT at 0 mM Na^+ ($P = 0.03$), but not 125 mM ($P = 0.235$).

significantly decreased basal [^{3}H]DA efflux from corresponding baseline ($P < 0.05$, post hoc Tukey's).

The pattern was similar but less pronounced in T62A-hDAT HEK cells even though the degree of [^{3}H]DA efflux was slightly lower than in WT (Fig. 7B). By two-way ANOVA, there was a significant effect of time [$P < 0.01$, ($F_{(3, 46)} = 5.391$)], and interaction of [Na^+_e] and time [$P < 0.0001$, $F_{(9, 46)} = 6.289$], but no significant effect of [Na^+_e] [$P = 0.0.476$, $F_{(3, 46)} = 0.842$]. The enhancement of [^{3}H]DA efflux elicited by low Na^+_e was most evident at the 5-minute time point. For clarity, statistical results for individual time periods are given in the legend to Fig. 7. As in WT-hDAT, AMPH significantly increased [^{3}H]DA efflux only at 50 mM and 125 mM Na^+_e. There was a tendency for AMPH to decrease [^{3}H]DA efflux at 0 mM Na^+_e as compared with the 15-minute baseline efflux at 0 mM Na^+_e; however, the difference was not statistically significant.

In T62D-hDAT HEK cells (Fig. 7C), a run-down in [^{3}H]DA efflux was visible as time progressed, but it was independent of Na^+_e. There was a significant effect of time by two-way ANOVA [$P < 0.0001$, $F_{(3, 51)} = 25.07$] but no interaction with time and [Na^+_e] and no main effect of [Na^+_e]. The decline in [^{3}H]DA efflux was not due to a loss of intracellular [^{3}H]DA, because 70–80% of the [^{3}H]DA originally taken up was still inside the cell after 20 minutes. AMPH does not induce [^{3}H]DA efflux at any [Na^+_e] in the T62D-hDAT mutant (Fig. 7C). All values at the 20-minute time point where AMPH was present were significantly different from values for 0 mM Na^+_e at 5 minutes and 10 minutes ($P < 0.05$ for both time points), but not 15 minutes, when all possible comparisons were made.

To better visualize the similarities or differences between T62D- and WT-hDAT, data for only these two constructs at 0 mM and 125 mM Na^+_e were graphed (Fig. 7D). In a general linear model three-way ANOVA, there was a significant effect of time versus cell type ($F = 10.277$, $df = 3$, $P = 0.0001$), a significant time versus sodium interaction ($F = 14.951$, $df = 3$, $P = 0.0001$), and a significant time versus cell type versus sodium interaction ($F = 10.190$, $df = 3$, $P = 0.0001$). There was no significant cell type versus sodium interaction ($P = 0.5$). At the initial 5-minute time point, [^{3}H]DA efflux in WT-hDAT was significantly elevated at 0 mM Na^+_e versus 125 mM Na^+_e ($P = 0.001$). Conversely, the level of [^{3}H]DA efflux is identical for T62D-hDAT at 0 and 125 mM Na^+_e ($P = 0.647$) and for WT at 0 mM Na^+_e ($P = 0.612$). Therefore, removal of Na^+_e transformed WT-hDAT into an efflux-favoring conformation that is simulated by T62D-hDAT independently of Na^+_e. [^{3}H]DA efflux in WT-hDAT remained stable between 5 and 15 minutes whether at 0 or 125 mM Na^+_e. On the contrary,

baseline [^{3}H]DA efflux in T62D-hDAT at both 0 and 125 mM Na^+_e began to decline within the first 10 minutes and the decrease was statistically significant at 15 minutes (see statistical values in legend for Fig. 7D). This decline continued even during the 5-minute incubation with 10 μM AMPH (20-minute point). The baseline efflux of [^{3}H]DA at 5 minutes in WT-hDAT at 0 mM Na^+_e was not statistically different from that elicited by 5 minutes of AMPH at 125 mm Na^+_e or the initial 5-minute Na^+_e-independent efflux observed in T62D-hDAT. From all the aforementioned interactions, we reasoned that the T62D-hDAT mutation produces a Na^+-primed state of the transporter that readily releases DA.

[^{3}H]DA efflux was sensitive to inhibition by 100 μM cocaine in all three DAT constructs. The fractional efflux of [^{3}H]DA in the presence of 100 μM cocaine was constant within each construct independent of time and [Na^+_e]. Fractional [^{3}H]DA release in the presence of 100 μM cocaine is 6.4 $\pm$ 0.1 for WT, 7.3 $\pm$ 0.6 for T62A-hDAT, and 4.9 $\pm$ 0.2 for T62D-hDAT ($n = 4$ each cell type, for all [Na^+_e]).

Discussion

This study provides evidence of differential regulation of DA uptake versus efflux functions in T62D-hDAT mutant; the disparity is accounted for by altered Na^+ regulation. A number of DAT mutants with restricted substrate influx have been identified, but few have been characterized for both forward and reverse transport. The DAT-Thr62 mutations are poised to provide key information concerning transporter conformational transitions. Despite striking differences in uptake and efflux behaviors for [^{3}H]DA, we found T62D-hDAT exhibited some characteristics identical to WT and to T62A-hDAT: membrane depolarization when expressed in *Xenopus* oocytes, uptake of the substrate ASP^+ when efflux was not a factor, and Na^+ concentration dependence of DA uptake. Despite its predilection to leak DA, T62D-hDAT assumes a conformation that confers normal uptake function and extracellular Na^+ binding. Whereas WT transporter requires Na^+ to reverse and expel DA, T62D-hDAT does not. T62D-hDAT appears to mimic a substrate- and Na^+-elicited conformation that normally permits reverse transport. The dual demonstration of normal DA uptake but constitutive efflux suggests T62D-hDAT is not fixed in position. Instead, T62D-hDAT may rapidly transition among the conformations for influx and efflux in sodium-dependent and -independent fashions, respectively.

Networks of molecular interactions drive substrate movement and transporter conformations. Thr62 is within a prime location to affect transporter orientation because of its proximity to TM1a, which forms part of the permeation pathway (Yamashita et al., 2005; Shan et al., 2011). TM1a is within an intracellular gating network (Kniazeff et al., 2008) that regulates DAT conformational transitions (Shan et al., 2011). Several DAT mutants, including T62D-hDAT, demonstrate particularly low DA inward transport. D345N-hDAT and Y335A-hDAT (Loland et al., 2002; Chen et al., 2004a) have been referred to as "inward-facing," meaning the transporter prefers a conformation in which the intracellular-facing gate is more accessible than the extracellular-facing gate. Intracellular interactions of these mutants have been characterized, lending credence to the inward-facing designation (Loland et al., 2004). We apply a similar description for the T62D-hDAT mutant (Guptaroy et al., 2009). Our study demonstrates that conformational transitions of the mutant are more complex than a simple inward- and outward-facing delineation.

The fluorescent substrate ASP^+ permitted interrogation of whether the Thr62-hDAT mutations truly disrupt the influx of substrate and, by inference, its intracellular retention. ASP^+ is well characterized as a substrate for both DAT and norepinephrine transporter (Schwartz et al., 2003). Once inside cells, ASP^+ is sequestered within mitochondria (Schwartz et al., 2003) and, as a noncatechol substrate, will not bind to the cytoplasmic side of the transporter to undergo outward transport (Liang et al., 2009). Identical ASP^+ accumulation in T62D- and WT-hDAT points to normal (outward-to-inward) translocation in T62D-hDAT. Therefore, the extremely low V_{max} of [^{3}H]DA in T62D-hDAT cells (Guptaroy et al., 2009) was attributable to continuous intracellular rebinding of [^{3}H]DA and its outward transport. This distinguishes T62D-hDAT from other DAT mutants characterized as inward facing (Loland et al., 2002; Chen et al., 2004a). The data also demonstrate T62A-hDAT takes up substrate identically to WT despite its V_{max} for DA uptake being about one-half of WT-hDAT (Guptaroy et al., 2009). Both influx and efflux functions of T62A-hDAT are compromised, but to a lower extent than T62D-hDAT (Guptaroy et al., 2009). The T62D-hDAT mutant shares similar characteristics to A559V-hDAT, a variant isolated from two male siblings with attention deficit–hyperactivity disorder (Mazei-Robison et al., 2008) and T356M-hDAT, a de novo mutation associated with autism spectrum disorder (Hamilton et al., 2013). Like T62D-, A559V-, and T356M-hDAT exhibit elevated baseline leak of DA and inhibition of outward efflux by AMPH (Mazei-Robison et al., 2008; Hamilton et al., 2013). The diminution of DA efflux by DA in WT-hDAT under low Na^+_e conditions, as observed in our study, was also noted by Pifl and Singer (1999).

Measurement of DAT currents indicate greater quantities of ions travel across the membrane than predicted (Sonders et al., 1997) by the stoichiometric ratio of 1:2:1 DA:Na^+:Cl^- (Rudnick, 1998). This implies a channel function of the transporter along with a substrate transport process. The similar depolarization exhibited in our DAT construct–expressing oocytes is probably the result of a common, substrate-independent leak current (Sonders et al., 1997). Conversely, profound differences in current conductance in *Xenopus* oocytes expressing WT- and T62D-hDAT were found when measured with substrate. No net current was detected in response to either DA or AMPH in T62D-hDAT oocytes. Absence of ion movement through T62D-hDAT is unlikely because the mutant exhibits normal Na^+-dependent substrate uptake. A net ion flux was restored in T62D-hDAT by the addition of Zn^{2+}. Zinc rescues influx in DAT mutants presenting drastically reduced DA uptake, such as Y335A-hDAT (Meinild et al., 2004) or D345N-hDAT (Chen et al., 2004a), and T62D-hDAT (Guptaroy et al., 2009). Here, Zn^{2+} enabled current measurement in the T62D-hDAT. Despite this restoration, there are diverse Zn^{2+} effects on various DAT mutants characterized as inward-facing, reflecting structural and conformation differences among the mutants that result in low substrate uptake. For instance, Zn^{2+} partly restored AMPH-induced DA efflux in T62D-hDAT-HEK cells (Guptaroy et al., 2009) but not in D345N-hDAT-HEK cells (Chen et al., 2004a).

Na^+ is a key determinant for the function of cotransporters. The electrophysiological phenotypes of WT- and T62D-hDAT oocytes in the presence and absence of substrate suggested the T62D mutation may affect Na^+ transport requirements. The interpretation that Thr62 mutations were primarily affecting transitions in the efflux pathway was strengthened by finding that the sodium requirement for DA influx was identical among the three DAT constructs. Reduction of the transmembrane Na^+ electrochemical gradient by either increasing intracellular Na^+ or reducing extracellular Na^+ inhibits neurotransmitter uptake but simultaneously promotes reverse transport (Raiteri et al., 1979; Liang and Rutledge, 1982; Khoshbouei et al., 2003; Zhen et al., 2005; Erreger et al., 2008) because of the build-up of Na^+ at the cytosolic face of the transporter (Raiteri et al., 1979; Liang and Rutledge, 1982). Khoshbouei et al. (2003) directly demonstrated this and proposed that AMPH-induced inward current increases intracellular Na^+ availability to DAT. T62D-hDAT, however, was insensitive to changes in the Na^+ electrochemical gradient such that reverse transport required no change in Na^+_e. This hints at the T62D-hDAT conformation existing in a Na^+-receptive orientation. Single-molecule fluorescence resonance energy transfer imaging of the Na^+-symporter DAT homolog LeuT at TM1a revealed two distinguishable states of the transporter in the absence of Na^+, consistent with two distinct conformations of the intracellular gate (Zhao et al., 2010, 2011). Addition of Na^+ or substrate decreased the transition frequency leading to preferential stabilization of an inward-closed state. Previous in silico modeling of T62D-hDAT in comparison with WT-hDAT indicated a disruption of a functionally important microenvironment, involving binding of T62 to other residues at the intracellular side (Guptaroy et al., 2009) and within an intracellular gating network (Kniazeff et al., 2008). Therefore, the T62D mutation can sustain multiple conformations of DAT, or lead to rapid interconversions of these conformations, with respect to the status of the inward-facing gate near TM1a. One conformation would permit normal Na^+ binding and influx whereas another orientation mimics the intracellular Na^+-primed state normally achieved as a result of AMPH action. We previously demonstrated that the K_m for [^{3}H]DA at the intracellular side of T62D-hDAT is significantly less than that of WT (Guptaroy et al., 2009). The Na^+-primed conformation of DAT readily rebinds DA, and it is unlikely that empty transporter returns to the surface. Thus, one of the conformations adopted by T62D-hDAT represents a Na^+-primed state that favors reverse transport.

The Na^+-sensitivity of other DAT mutants has not been routinely measured. The A559V-hDAT variant demonstrated an enhanced sensitivity but remained responsive to intracellular Na^+ (Mazei-Robison et al., 2008). T62D-hDAT was unresponsive to partial, indirect changes in the transmembrane Na^+ gradient via extracellular Na^+ substitution. Nonetheless, the similarities underscore the importance of the sodium gradient in maintaining conformational states of DAT.

This study revealed novel attributes of hDAT Thr62 mutations, particularly in mutation of Thr62 to aspartate. This mutation makes evident that DAT exists in conformations that exhibit normal substrate uptake with unregulated efflux. T62A-hDAT is a less severe mutation, showing reduced sensitivity to AMPH but not the overtly unregulated efflux attained by T62D-hDAT. T62D-hDAT binds Na^+ and transports DA inward normally but has lost the capacity for intracellular Na^+ to stimulate shifts in transporter orientation. Taken together, our data place importance on the molecular interactions between residues involving Na^+ differentially influencing the efflux properties of the transporter. The T62D-hDAT and other transporter mutants can serve as informational experimental models for changes that occur to the transporter after exposure to AMPH.

Acknowledgments

The authors thank Dr. Asim Beg (University of Michigan) for the pSGEM oocyte construct and initial help with *Xenopus* oocyte studies. They are grateful to Dr. Samuel Straight at the Center for Live Cell Imaging for initial consultation and assistance with confocal image analysis. They also appreciate the statistical analyses of three-way interactions provided by Felicia R. Webb at the University of Michigan. They acknowledge the University of Michigan Pharmacology Department confocal microscopy facility and the DNA Sequencing Core. Lastly, they thank Sarah Mikelman for technical assistance.

Authorship Contributions

Participated in research design: Fraser, Chen, DeFelice, Gnegy.

Conducted experiments: Fraser, Chen, Luderman, Stokes.

Contributed new reagents or analytic tools: Fraser, Chen, Guptaroy, Beg.

Performed data analysis: Fraser, Chen, DeFelice, Gnegy.

Wrote or contributed to the writing of the manuscript: Fraser, Chen, DeFelice, Gnegy.

References

Carvelli L, Blakely RD, and DeFelice LJ (2008) Dopamine transporter/syntaxin 1A interactions regulate transporter channel activity and dopaminergic synaptic transmission. *Proc Natl Acad Sci USA* **105**:14192–14197.

Carvelli L, McDonald PW, Blakely RD, and Defelice LJ (2004) Dopamine transporters depolarize neurons by a channel mechanism. *Proc Natl Acad Sci USA* **101**: 16046–16051.

Chen N, Rickey J, Berfield JL, and Reith ME (2004a) Aspartate 345 of the dopamine transporter is critical for conformational changes in substrate translocation and cocaine binding. *J Biol Chem* **279**:5508–5519.

Chen, NH, Reith, ME, and Quick, MW (2004b). Synaptic uptake and beyond: the sodium- and chloride-dependent neurotransmitter transporter family SLC6. *Pflugers Arch.* 447:519–531.

DeFelice LJ and Goswami T (2007) Transporters as channels. *Annu Rev Physiol* **69**: 87–112.

Erreger K, Grewer C, Javitch JA, and Galli A (2008) Currents in response to rapid concentration jumps of amphetamine uncover novel aspects of human dopamine transporter function. *J Neurosci* **28**:976–989.

Foster JD, Pananusorn B, and Vaughan RA (2002) Dopamine transporters are phosphorylated on N-terminal serines in rat striatum. *J Biol Chem* **277**: 25178–25186.

Foster JD, Yang JW, Moritz AE, Challasivakanaka S, Smith MA, Holy M, Wilebski K, Sitte HH, and Vaughan RA (2012) Dopamine transporter phosphorylation site threonine 53 regulates substrate reuptake and amphetamine-stimulated efflux. *J Biol Chem* **287**:29702–29712.

Guptaroy B, Zhang M, Bowton E, Binda F, Shi L, Weinstein H, Galli A, Javitch JA, Neubig RR, and Gnegy ME (2009) A juxtamembrane mutation in the N terminus of the dopamine transporter induces preference for an inward-facing conformation. *Mol Pharmacol* **75**:514–524.

Guptaroy B, Fraser R, Desai A, Zhang M, and Gnegy ME (2011) Site-directed mutations near transmembrane domain 1 alter conformation and function of norepinephrine and dopamine transporters. *Mol Pharmacol* **79**:520–532.

Hahn MK and Blakely RD (2007) The functional impact of SLC6 transporter genetic variation. *Annu Rev Pharmacol Toxicol* **47**:401–441.

Hamilton PJ, Campbell NG, Sharma S, Erreger K, Herborg Hansen F, Saunders C, Belovich AN, Sahai MA, Cook EH, and Gether U et al.; NIH ARRA Autism Sequencing Consortium (2013) De novo mutation in the dopamine transporter gene associates dopamine dysfunction with autism spectrum disorder. *Mol Psychiatry* **18**:1315–1323.

Ingram SL, Prasad BM, and Amara SG (2002) Dopamine transporter-mediated conductances increase excitability of midbrain dopamine neurons. *Nat Neurosci* **5**: 971–978.

Jardetzky O (1966) Simple allosteric model for membrane pumps. *Nature* **211**: 969–970.

Khoshbouei H, Wang H, Lechleiter JD, Javitch JA, and Galli A (2003) Amphetamine-induced dopamine efflux. A voltage-sensitive and intracellular Na+-dependent mechanism. *J Biol Chem* **278**:12070–12077.

Khoshbouei H, Sen N, Guptaroy B, Johnson L, Lund D, Gnegy ME, Galli A, and Javitch JA (2004) N-terminal phosphorylation of the dopamine transporter is required for amphetamine-induced efflux. *PLoS Biol* **2**:E78.

Kniazeff J, Shi L, Loland CJ, Javitch JA, Weinstein H, and Gether U (2008) An intracellular interaction network regulates conformational transitions in the dopamine transporter. *J Biol Chem* **283**:17691–17701.

Krishnamurthy H and Gouaux E (2012) X-ray structures of LeuT in substrate-free outward-open and apo inward-open states. *Nature* **481**:469–474.

Levi G and Raiteri M (1993) Carrier-mediated release of neurotransmitters. *Trends Neurosci* **16**:415–419.

Leviel V (2011) Dopamine release mediated by the dopamine transporter, facts and consequences. *J Neurochem* **118**:475–489.

Liang NY and Rutledge CO (1982) Evidence for carrier-mediated efflux of dopamine from corpus striatum. *Biochem Pharmacol* **31**:2479–2484.

Liang YJ, Zhen J, Chen N, and Reith ME (2009) Interaction of catechol and noncatechol substrates with externally or internally facing dopamine transporters. *J Neurochem* **109**:981–994.

Loland CJ, Norregaard L, Litman T, and Gether U (2002) Generation of an activating Zn(2+) switch in the dopamine transporter: mutation of an intracellular tyrosine constitutively alters the conformational equilibrium of the transport cycle. *Proc Natl Acad Sci USA* **99**:1683–1688.

Loland CJ, Grånäs C, Javitch JA, and Gether U (2004) Identification of intracellular residues in the dopamine transporter critical for regulation of transporter conformation and cocaine binding. *J Biol Chem* **279**:3228–3238.

Mazei-Robison MS, Bowton E, Holy M, Schmudermaier M, Freissmuth M, Sitte HH, Galli A, and Blakely RD (2008) Anomalous dopamine release associated with a human dopamine transporter coding variant. *J Neurosci* **28**:7040–7046.

Meinild AK, Sitte HH, and Gether U (2004) Zinc potentiates an uncoupled anion conductance associated with the dopamine transporter. *J Biol Chem* **279**:49671–49679.

Pifl C, Agneter E, Drobny H, Reither H, and Singer EA (1997) Induction by low Na+ or Cl- of cocaine sensitive carrier-mediated efflux of amines from cells transfected with the cloned human catecholamine transporters. *Br J Pharmacol* **121**:205–212.

Pifl C and Singer EA (1999) Ion dependence of carrier-mediated release in dopamine or norepinephrine transporter-transfected cells questions the hypothesis of facilitated exchange diffusion. *Mol Pharmacol* **56**:1047–1054.

Raiteri M, Cerrito F, Cervoni AM, and Levi G (1979) Dopamine can be released by two mechanisms differentially affected by the dopamine transport inhibitor nomifensine. *J Pharmacol Exp Ther* **208**:195–202.

Rudnick G (1998) Ion-coupled neurotransmitter transport: thermodynamic vs. kinetic determinations of stoichiometry. *Methods Enzymol* **296**:233–247.

Schwartz JW, Blakely RD, and DeFelice LJ (2003) Binding and transport in norepinephrine transporters. Real-time, spatially resolved analysis in single cells using a fluorescent substrate. *J Biol Chem* **278**:9768–9777.

Shan J, Javitch JA, Shi L, and Weinstein H (2011) The substrate-driven transition to an inward-facing conformation in the functional mechanism of the dopamine transporter. *PLoS ONE* **6**:e16350.

Solis E, Jr, Zdravkovic I, Tomlinson ID, Noskov SY, Rosenthal SJ, and De Felice LJ (2012) 4-(4-(dimethylamino)phenyl)-1-methylpyridinium (APP+) is a fluorescent substrate for the human serotonin transporter. *J Biol Chem* **287**:8852–8863.

Sonders MS, Zhu SJ, Zahniser NR, Kavanaugh MP, and Amara SG (1997) Multiple ionic conductances of the human dopamine transporter: the actions of dopamine and psychostimulants. *J Neurosci* **17**:960–974.

Sulzer D, Sonders MS, Poulsen NW, and Galli A (2005) Mechanisms of neurotransmitter release by amphetamines: a review. *Prog Neurobiol* **75**:406–433.

Vaughan RA (2004) Phosphorylation and regulation of psychostimulant-sensitive neurotransmitter transporters. *J Pharmacol Exp Ther* **310**:1–7.

Yamashita A, Singh SK, Kawate T, Jin Y, and Gouaux E (2005) Crystal structure of a bacterial homologue of Na+/Cl—dependent neurotransmitter transporters. *Nature* **437**:215–223.

Zapata A, Kivell B, Han Y, Javitch JA, Bolan EA, Kuraguntla D, Jaligam V, Oz M, Jayanthi LD, and Samuvel DJ et al. (2007) Regulation of dopamine transporter function and cell surface expression by D3 dopamine receptors. *J Biol Chem* **282**:35842–35854.

Zhao Y, Terry D, Shi L, Weinstein H, Blanchard SC, and Javitch JA (2010) Single-molecule dynamics of gating in a neurotransmitter transporter homologue. *Nature* **465**:188–193.

Zhao C, Stolzenberg S, Gracia L, Weinstein H, Noskov S, and Shi L (2012) Ion-controlled conformational dynamics in the outward-open transition from an occluded state of LeuT. *Biophys J* **103**:878–888.

Zhao Y, Terry DS, Shi L, Quick M, Weinstein H, Blanchard SC, and Javitch JA (2011) Substrate-modulated gating dynamics in a Na+-coupled neurotransmitter transporter homologue. *Nature* **474**:109–113.

Zhen J, Chen N, and Reith ME (2005) Differences in interactions with the dopamine transporter as revealed by diminishment of Na(+) gradient and membrane potential: dopamine versus other substrates. *Neuropharmacology* **49**:769–779.

Address correspondence to: Dr. Margaret E. Gnegy, Department of Pharmacology, 2220E MSRBIII, University of Michigan Medical School, 1150 West Medical Center Drive, Ann Arbor, MI 48109-0632. E-mail: pgnegy@umich.edu